Investigations of Bearing Failures Associated with White Etching Areas (WEAs) in Wind Turbine Gearboxes

Robert Errichello, Robert Budny and Rainer Eckert

A critical problem for wind turbine gearboxes is failure of rolling element bearings where axial cracks form on the inner rings. This article presents field experience from operating wind turbines that compares the performance of through-hardened and carburized materials. It reveals that through-hardened bearings develop WEA/WECs and fail with axial cracks, whereas carburized bearings do not. The field experience further shows that a carburized bearing with a core having low carbon content, high nickel content, greater compressive residual stresses, and a higher amount of retained austenite provides higher fracture resistance and makes carburized bearings more durable than through-hardened bearings in the wind turbine environment.

Introduction

Microstructural alterations have been studied since 1947 (Ref. 1): From the late 1960s through the 1980s, classic, subsurface-initiated fatigue was investigated (Refs. 2 – 9), including the well-documented, slow, structural breakdown (martensite decay) — a progressive change in the steel matrix that occurs under moderately high Hertzian stresses. The decay creates dark etching areas followed by white etching bands (Ref. 1). Flat white bands (WBs) first form at an angle of 30 – 40° to the surface (Refs. 1, 7), and steep WBs form later at an angle of 70 – 80° to the surface (Refs. 1, 7). Steep bands are located closer to the surface in the area of the greatest density of the flat WBs. Hertzian stress and the number of cycles are the controlling parameters for dark etching areas and WBs. And as the number of load cycles increase, 1) the hardness drops in areas of structural changes; 2) the hardness minima displace toward the surface; and 3) the X-ray diffraction half-value breadth decreases (Refs. 1, 3, 7). The Hertzian stress limit for the development of WBs is $p_o \sim 2{,}500$ MPa (Refs. 1, 7).

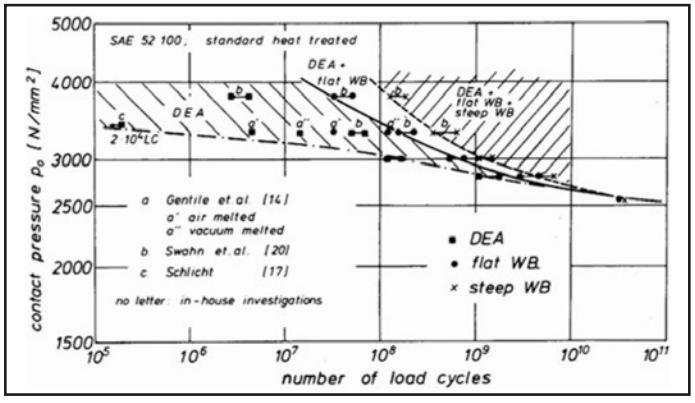

Figure 1 Correlation between Hertzian stress, load cycles and microstructural alterations (Ref. 6).

WBs consist of nanosized, ferrite cellular structures that — due to their fine-grained, cellular structure — have a hardness that is 30 – 50% higher than the hardness of the surrounding matrix (Refs. 10 – 13).

When residual stresses are superimposed on Hertzian stresses, it is found that flat WBs are perpendicular to the effective tensile stress, and steep WBs coincide with the direction of the maximum shear stress (Ref. 7).

Figure 1 shows that it is possible to draw conclusions about the Hertzian stress that was effective at the time of formation of WBs from the position, density, and direction of the WBs (Ref. 7).

WEA Morphology and Characteristics of Butterflies

Stress concentrations occur around inhomogeneities (nonmetallic inclusions and large carbides) due to elastoplastic strain incompatibility between the inhomogeneities and the martensitic matrix (Ref. 14). Once the yield strength of the matrix is exceeded, a plastic strain is induced in a small domain surrounding the inhomogeneities. Under repeated Hertzian stress dislocations shuttle back and forth and accumulate in this domain. This process causes localized changes in microstructure — such as white etching areas (WEAs) — with what look like "butterfly wings." Cracks nucleate in this domain once a critical density of dislocations is reached. The origin of a subsurface-initiated macropit most often occurs at the depth of the maximum, orthogonal alternating shear stress — and which is the basis of the Lundberg-Palmgren theory for rating bearing life.

WEAs with the appearance of butterflies form adjacent to nonmetallic inclusions in planes 40 – 50° from the surface, corresponding to planes of maximum, unidirectional shear stresses (Refs. 1, 3, 15). According to References 11 and 16, butterflies form with AISI 52100 steel when the maximum shear stress $\tau_{max} > 400$ MPa.

No simple relationship between Hertzian stress and microcracks exists because the relationship is related to applied stress, local matrix conditions and the composition, shape, size and alignment of the inclusion with the stress field (Ref. 11).

Heat treatment conditions do not significantly affect butterfly development. However, inclusion type, inclusion size, inclusion distribution and forging reduction ratio do (Ref. 11). Well-dispersed, small spherical inclusions ($< 13\,\mu m$) and high forging reduction ratios ($\geq 7{:}1$) maximize resistance to cracks associated with butterflies (Ref. 11).

Plate-like (lenticular) carbides are thin, carbide discs sandwiched between WEAs (Refs. 1, 3); lenticular carbides appear dark black on etching (Refs. 1, 3).

WEAs will increase in number with longer cycling time. Their density varies in a manner consistent with the variation in shear stress, and WEAs form at a rapid rate around nonmetallic inclusions (Ref. 3). The maximum density of WEAs occurs at the depth of the maximum, unidirectional shear stress (Ref. 3).

Butterflies are the result of an accumulation of localized plastic deformation at inhomogeneities, such as non-metallic inclusions and large carbides (Refs. 14, 17).

Cracks tend to propagate along the boundary of WEAs; yet it is not resolved whether WEAs precede cracking (Ref. 17) or cracking precedes WEAs (Refs. 12, 15, 18).

Many microcracks are nucleated at inclusion butterflies early in the fatigue life, but most do not grow beyond the WEAs unless the inclusions are located at Hertzian depths where the cyclic shear stress is high (Refs. 11and 12).

Transmission electron microscope investigations (Refs. 10, 17) show that WEAs consist of ultrafine, nanocrystalline ferrite grains. Researchers (Refs. 10, 11) concluded that WEAs result from recrystallization, where new grains grow from a highly deformed steel matrix.

Though WEAs have been the subject of considerable study, there has been no clear link between WEAs and Hertzian fatigue. Grabulov (Ref. 10) and others have found that the microstructure of classic, subsurface-initiated macropitting is very different from the WEAs observed at inclusion butterflies. Therefore, WEAs are not an essential step in classic subsurface-initiated macropitting.

WEAs are not limited to wind turbine gearbox bearings; they occur in many other industries as well (Refs. 12, 16, 19, 20). Furthermore, WEAs are not limited to any one gear manufacturer, bearing manufacturer, or wind turbine manufacturer (Refs. 16, 19, 20, 21).

Currently, there is no calculation method that is recognized for predicting WEAs, and the root cause and significance of WEAs are not clearly understood (Refs. 13, 16, 19, 20, 21, 22, 24, 25).

Morphology and Characteristics of Irregular White Etching Areas and White Etching Cracks

An immediate, critical problem for wind turbine gearboxes is a failure of rolling element bearings in which axial cracks form on the inner rings. Metallurgical analyses show that the failure mode is associated with microstructural alterations manifested by irregular white etching areas (irWEAs) and white etching cracks (WECs). IrWEAs are branching crack networks that follow pre-austenite grain boundaries and form crack networks with white etching borders. WECs can be straight-growing cracks that are parallel to the surface, or branching crack networks (Ref. 12), i.e. — irWEAs. Both are associated with axial cracks in wind turbine bearings. There are several hypotheses for the root cause of irWEAs, WECs and axial cracks, including impact loads (Ref. 13, 19, 20, 22); sliding (Refs. 16, 19, 22); hydrogen embrittlement (Refs. 16, 18, 21); electrostatic discharge (Refs. 19, 21); corrosion fatigue (Ref. 16), and adiabatic shear (Ref. 20). However, none of the hypotheses has been proven, and it is currently an active field of research (Refs. 13, 16, 19, 20, 21, 22).

It is known that WBs, WECs and irWEAs share similar, microstructural morphologies. They are nanosized, ferrite cellular structures that result from recrystallization of new grains that grow from the highly deformed steel matrix. Therefore WBs, WECs and irWEAs are in fact different development stages of the same phenomenon (Ref. 11).

How irWEAs and WECs develop and progress is not yet understood — both have been characterized as brittle fracture modes that generate cleavage fractures. It might be a single-step or a multiple-step process that generates cleavage cracks and WBs (Refs. 13, 16, 19, 20, 21, 22).

It is also not yet understood how a chemical conversion coating such as black oxide helps to prevent irWEAs and axial cracks. It might reduce tractional stresses, damp vibrations, or prevent hydrogen diffusion. On the other hand, the temperatures used to treat the components might beneficially alter the bearing metallurgy (Refs. 16, 19, 20, 22).

We usually do not find moisture corrosion, severe wear, or electric discharge damage in wind turbine gearboxes. Therefore, hydrogen absorption due to water in oil can be excluded and hydrogen generation due to sliding or electric discharge and diffusion into the bearing seems unlikely. Furthermore, although the authors have seen butterflies in wind turbine bearings, there is little evidence to support butterfly cracks propagating into irWEAs or WEC networks.

Description of Wind Turbine Bearing Failures

In the following sections we present actual field experience with active wind turbines that compares the performance of rolling element bearings manufactured from both through-hardened and carburized materials. The wind turbines are utility-scale and have been operating for up to six years; There are over 500 turbines of this type currently in operation.

Through-hardened vs. carburized intermediate bearings. The wind turbine utilizes an NJ 2334 cylindrical roller bearing at each end of the four intermediate (INT) shafts in the gearbox. The bearings are manufactured by two different manufacturers, designated here as bearings INT–A and INT–B. The INT–B bearing is through-hardened and the INT–A bearing is carburized. The failure rate of the INT–B through-hardened bearings is 16%, with a mean time-to-failure rate of 27,200 h (1.4×10^8 cycles). To date, there has been only one failure of an INT–A carburized bearing, and that single failure is believed to be of a secondary nature that occurred due to the presence of a surface defect of unknown origin.

Table 1 compares data for the INT bearings and Table 2 compares chemistry for the INT bearings.

Figures 2a and 2b show a failed INT–B bearing inner ring (IR) that had operated for 18,000 h (9.3×10^7 cycles) when the failure was discovered. There are numerous axial cracks concentrated toward the flange end of the IR. Figure 3 is a micrograph of a circumferential metallurgical section through an axial crack. The section has been nital-etched to display the irWEAs associated with the crack. Figure 4 is a scanning electron microscope image of an axial crack that was opened in the laboratory to expose the fracture surface. The crack morphology is typical of axial cracks found on through-hardened bearings from wind turbines (Refs. 13, 16, 19, 20, 21, 22). The origin of the fracture is believed to be at the center of the smooth circular "lens" (Ref. 16).

Residual stresses and retained austenite were measured on new, unused intermediate bearings. Figure 5 shows residual stresses on INT bearings determined by X-ray diffraction (XRD), per ASTM E915. The residual stress for the INT–B through-hardened bearing is compressive up to –700 MPa at the surface, decreases to zero at a depth of 12 μm, and is tensile (ranging from 35 – 100 MPa) at depths greater than 13 μm. The residual stress for the INT–A carburized bearing is entirely compressive up to –1,000 MPa at the surface, and greater than –400 MPa to a depth of 500 μm.

Figure 6 shows retained austenite on INT bearings determined by XRD, per ASTM E975. The retained austenite for the INT–B through-hardened bearing is less than 1%. The retained austenite for the INT–A carburized bearing ranges from 23 – 31%.

Carburized rotor bearings. The wind turbine utilizes a tapered roller bearing at each end of the rotor shaft. The bearings are manufactured by two different manufacturers, designated here as bearings ROT–C and ROT–D; both are car-

Table 1 Data for intermediate bearings

Parameter	INT-A	INT-B
Bore, *d* (mm)	170	170
Outside diameter, *D* (mm)	360	360
Width, *T* (mm)	120	120
Dynamic capacity, *C* (kN)	1,840	1,660
Static capacity, C_o (kN)	2,110	2,040
Fatigue limit load, P_u (kN)	332	204
Number of rollers, *z*	14	14
Roller pitch diameter, *Dpw* (mm)	268	266
Roller mean diameter, D_w (mm)	52	50
Roller total length, l_w (mm)	85	85
Roller effective length, l_{weff} (mm)	81	81
Roller crown type	Circular	End reliefs
Roller crown magnitude (mm)	0.030	0.036
Nominal contact angle, α_o (°)	0	0
Heat treatment	Carburized	Through-hardened
IR case depth, E_{hr} (mm)	3.5	N/A
Cage type	Brass	Brass
Hertzian stress (MPa)	1,583	1,756
Hertzian stress max (MPa)	1,869	2,056
Shaft speed (rpm)	86.12	86.12
DIN ISO 281-4 life (h)	212,200	178,500

Table 2 Chemical composition for intermediate bearings

Element	INT-A IR (% wt.)	INT-B IR (% wt.)
Carbon, C	0.227	1.02
Silicon, Si	0.288	0.270
Manganese, Mn	0.774	0.280
Chromium, Cr	0.660	1.69
Nickel, Ni	1.67	0.130
Molybdenum, Mo	0.226	0.210
Sulfur, S	0.017	0.013
Phosphorus, P	0.010	0.015
Copper, Cu	0.190	0.260
Aluminum, Al	0.045	Not reported
Cobalt, Co	0.019	Not reported
Columbium, Cb	0.011	Not reported
Titanium, Ti	0.005	Not reported
Boron, B	<0.001	Not reported
Vanadium, V	0.006	Not reported
Tin, Sn	0.005	Not reported

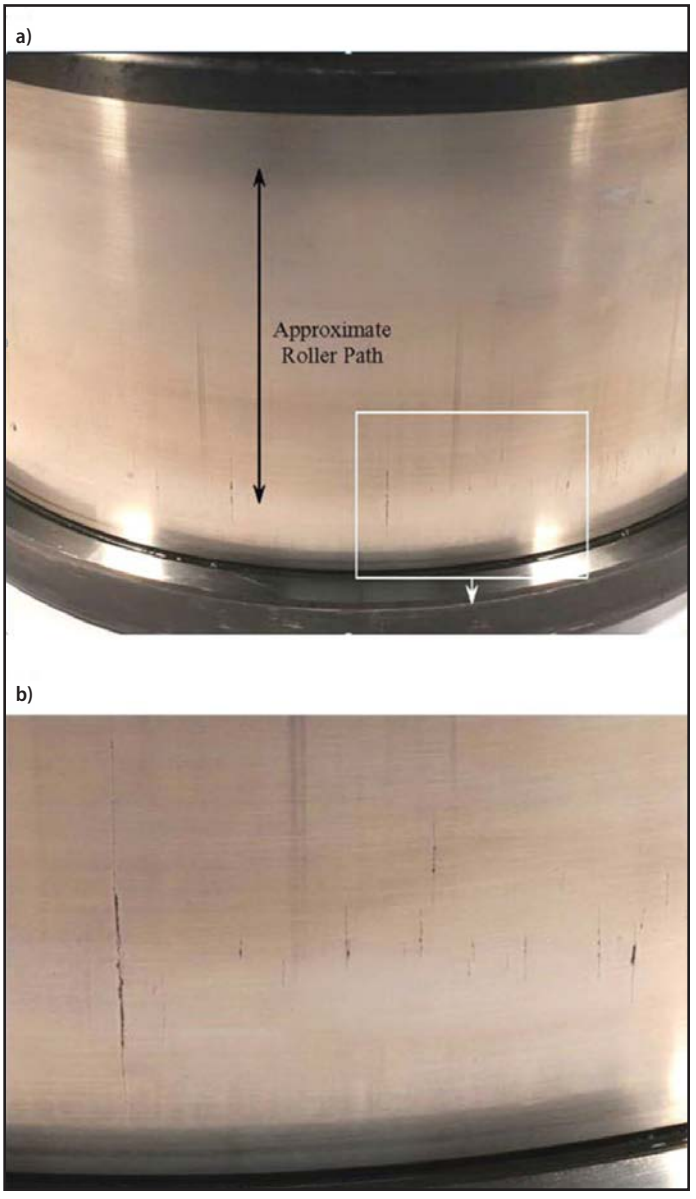

Figure 2 (a) Axial cracks on intermediate bearing INT–B IR; (b) axial cracks on intermediate bearing INT–B IR.

burized. The failure rate of the ROT–D bearings is 17%, with a mean time-to-failure of 26,690 h (2.2×10^7 cycles). As this article is written, there have been no failures of a ROT–C bearing.

Table 3 compares data for the rotor bearings; Table 4 compares chemistry for the rotor bearings.

Figure 3 Irregular white etching areas on axial crack.

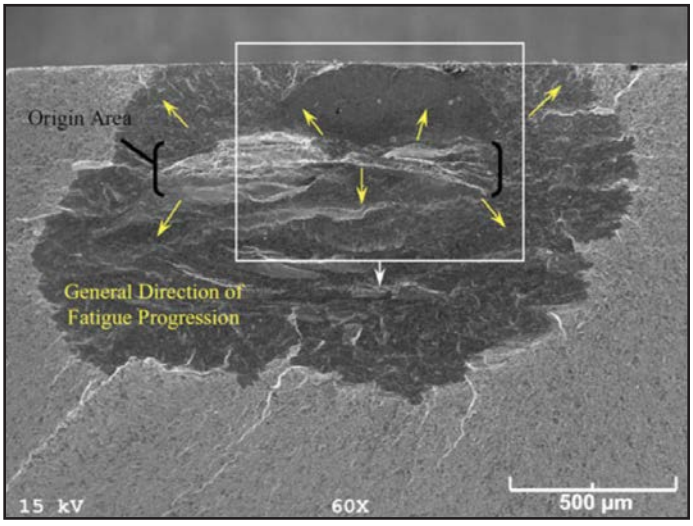

Figure 4 Opened axial crack on intermediate bearing INT–B IR.

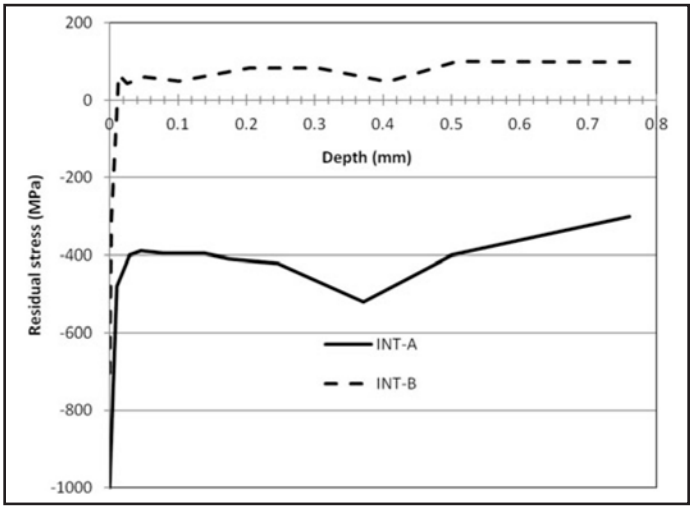

Figure 5 Residual stresses for intermediate bearings.

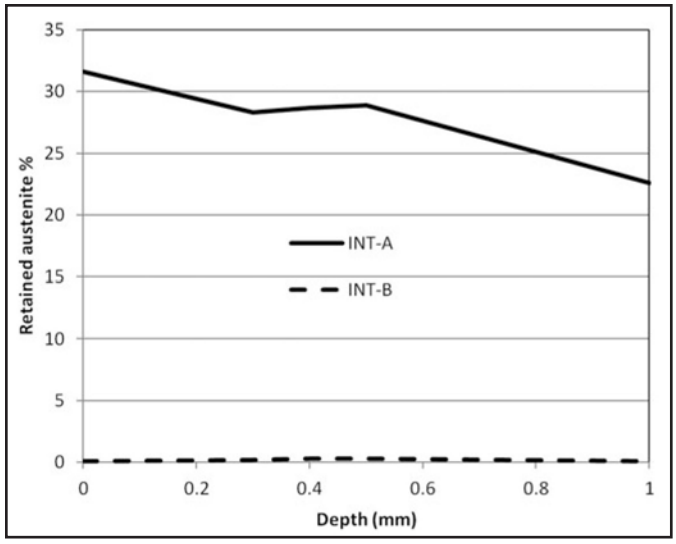

Figure 6 Retained austenite for intermediate bearings.

Table 3 Data for rotor bearings

Parameter	ROT-C	ROT-D
Bore, d (mm)	749.3	749.3
Outside diameter, D (mm)	990.6	990.6
Width, T (mm)	159.5	159.5
Dynamic capacity, C (kN)	4,460	5,330
Static capacity, C_o (kN)	13,200	13,110
Fatigue limit load, P_u (kN)	1,477	1,467
Number of rollers, z	43	43
Roller pitch diameter, D_{pw} (mm)	868.2	869.95
Roller mean diameter, D_w (mm)	58.5	60.15
Roller total length, l_w (mm)	118.1	118.1
Roller effective length, l_{weff} (mm)	114.1	107.1
Roller crown type	Circular	End reliefs
Roller crown magnitude (mm)	0.030	0.053
Nominal contact angle, α_o (°)	12.5	12.5
Axial preload, G_{ao} (mm)	0.2	0.3
Heat treatment	Carburized	Carburized
IR case depth, E_{hr} (mm)	3.5	3.5
Cage type	Stamped	Pinned
Hertzian stress (MPa)	1,634	1,798
Hertzian stress max (MPa)	1,886	2,075
Shaft speed (rpm)	13.66	13.66
DIN ISO 281-4 life (h)	146,000	121,300

Table 4 Chemical composition for rotor bearings

Element	ROT-C IR (% wt.)	ROT-D IR (% wt.)
Carbon, C	0.126	0.199
Silicon, Si	0.217	0.265
Manganese, Mn	0.405	0.453
Chromium, Cr	1.29	1.32
Nickel, Ni	3.30	3.44
Molybdenum, Mo	0.099	0.190
Sulfur, S	0.016	0.003
Phosphorus, P	0.013	0.009
Copper, Cu	0.218	0.130
Aluminum, Al	0.030	0.029
Cobalt, Co	0.017	0.018
Columbium, Cb	0.013	< 0.001
Titanium, Ti	0.005	< 0.001
Boron, B	< 0.001	< 0.001
Vanadium, V	0.008	< 0.001
Tin, Sn	0.023	0.018

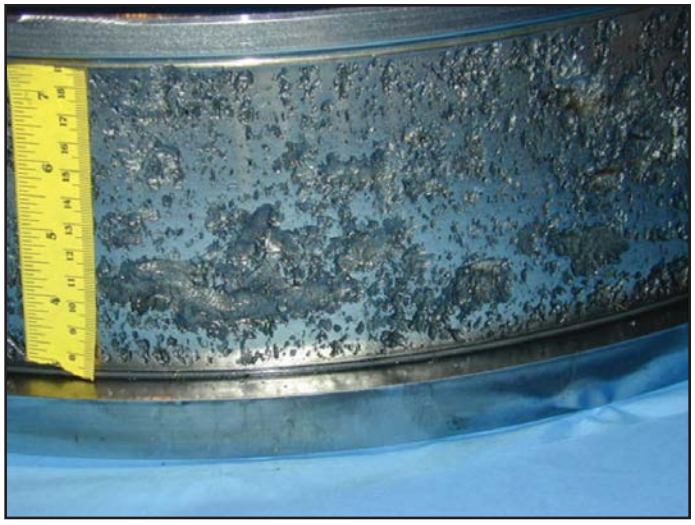

Figure 7 Macropitting on rotor bearing ROT–D IR.

a)

b)

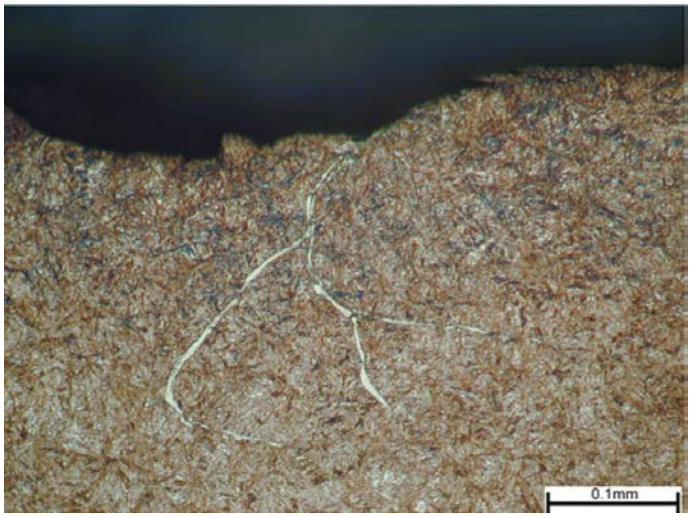

Figure 8 (a) Macropits and irWEAs on rotor bearing ROT–D IR; (b) macropits and irWEAs on rotor bearing ROT–D IR.

Figure 7 shows a failed ROT–D rotor bearing — IR — that had operated for 22,000 h (1.8×10^7 cycles) when the failure was discovered. The entire circumference of the IR is covered with severe macropitting.

Figure 8a is a micrograph of a circumferential, metallurgical section through a macropit. The section has been nital-etched to display the irWEAs associated with the macropits. Figure 8b is at a higher magnification and shows cracks within the irWEAs. The crack morphology is typical of macropitting found on carburized bearings from wind turbines (Refs. 12, 13, 19).

Residual stresses and retained austenite were measured on new, unused rotor bearings. Figure 9 shows residual stresses on rotor bearings determined by XRD, per ASTM E915. The residual stresses for the ROT–C and ROT–D bearings are entirely compressive to a depth of 500 μm. For depths below 20 μm, the residual stress for the ROT–D bearing is –250 MPa near the surface, and it fades to zero IMPa at a depth of 500 μm; whereas the residual stress for the ROT–C bearing increases from –250 MPa near the surface to a maximum of –350 MPa at a depth of 300 μm and fades to –100 MPa at a depth of 500 μm.

Figure 10 shows retained austenite on rotor bearings determined by XRD, per ASTM E975. The retained austenite for the ROT–D bearing ranges from 12 – 17%; the retained austenite for the ROT–C bearing ranges from 20 – 26%.

Two non-failing rotor bearings (a ROT–C and a ROT–D) were removed from service after 25,000 h and metallurgically examined. The ROT–C bearing had butterflies at depths ranging from 100 – 400 μm, but *no* irWEAs. The ROT–D bearing had numerous irWEAs at depths ranging from 400 – 600 μm (Fig. 11).

Discussion

The wind turbine gearbox failures have shown that through-hardened bearing failure is caused by axial cracks, whereas carburized bearing failure is due to macropitting. This is consistent with the findings of other investigators (Refs. 16, 19, 20, 22).

Through-hardened vs. carburized intermediate bearings. Table 1 shows that the INT–A and INT–B bearings have similar geometries. However, Table 2 also shows that the INT–B through-hardened bearing and INT–A carburized bearing have very different chemistries. Furthermore, Figures 5 and 6 show that the INT–B through-hardened bearings have tensile residual stresses and very little retained austenite, whereas the INT–A carburized bearings have significantly higher compressive, residual stresses and greater amounts of retained austenite.

To compare the properties of the bearings to other industries, the evolution of bearing materials for gas turbines has shown that a carburized bearing with a core having a low-carbon, high-nickel content — such as M50NiL (Ref. 23) — has a relatively high fracture resistance compared to an M50 through-hardened bearing. Furthermore, Forster (Ref. 23) found WEAs in AISI 52100 and AISI M50 bearings — but no WEAs in M50NiL bearings.

Figure 4 shows that the origin of the brittle fracture lens is about 300 μm below the surface. Figure 5 shows that the residual stress at this depth is about +85 MPa tensile for the INT–B through-hardened bearing, and about –450 MPa com-

pressive for the INT–A carburized bearing. We believe that the compressive, residual stress increases fracture resistance and is the principal reason the INT–A carburized bearing is immune to axial cracks.

In summary, the intermediate bearings have similar geometry but very different chemistry, residual stresses, and retained austenite. Therefore, it is believed that the better performance of the INT–A carburized bearing is due to different chemistry with a core having a low-carbon, high-nickel content; greater compressive residual stress; and a higher amount of retained austenite. All of these properties provide higher fracture resistance and make carburized bearings more durable in the wind turbine environment than through-hardened bearings.

Carburized rotor bearings. Tables 3 and 4 show that the ROT–C and ROT–D rotor bearings have similar geometries and chemistries. Yet Figure 10 shows that the ROT–C bearings have a significantly greater amount of retained austenite — at *all* depths. Furthermore, metallurgical analyses of non-failing bearings have shown that no irWEAs form in the ROT–C bearing, whereas irWEAs form in the ROT–D bearing at depths ranging from 400 to 600 μm (Fig. 11). Figure 9 shows that the residual stresses for the ROT–C and ROT–D bearings are very similar at the depths of the irWEAs. In summary, the carburized rotor bearings ROT–C and ROT–D have similar macrogeometries, chemistries, and residual compressive stresses — *but different levels of retained austenite*. There are also differences in the design roller profiles between the two bearings, and analysis of the profiles predicts higher peak stress for the ROT–D profile under many operating conditions. Furthermore, coordinate measuring machine (CMM) measurements made on actual components suggest that the as-built roller geometry of ROT–D bearings results in even higher peak stress under many operating conditions than do the nominal profiles. It is therefore believed that the better performance of ROT–C bearings is due to their higher amount of retained austenite, superior roller profile design, and reduced variation in manufacturing.

Through-Hardened vs. Carburized Bearing Performance: A Summary

The authors' experience shows that through-hardened bearings display irWEAs on axial cracks that propagate radially through the bearing IR section (Fig. 3), whereas carburized bearings display irWEAs on crack networks that occur over large, subsurface areas at depths ranging from near the surface to the depth of the maximum shear stress (Fig. 11). Eventually the cracks reach the surface, where they form macropits; this is consistent with the findings of other investigators (Refs. 16, 20, 22). This failure mode is sometimes known as "white structure flaking (Ref. 21)."

The authors' experience, and that of others — (Refs. 15, 20, 22) — has shown that carburized bearings *with a proper microstructure* can be immune to the axial crack failure mode and are more durable in a wind turbine environment than through-hardened bearings. Furthermore, the authors' results show that if the carburized microstructure has at least 20% retained austenite, irWEAs do not form and premature macropitting is avoided.

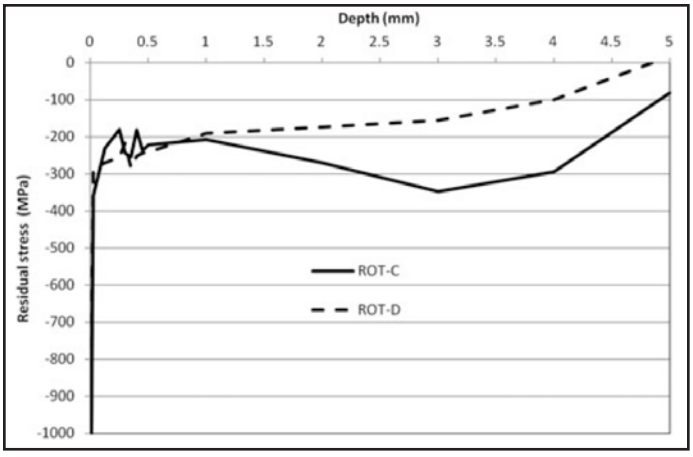

Figure 9 Residual stresses for rotor bearings.

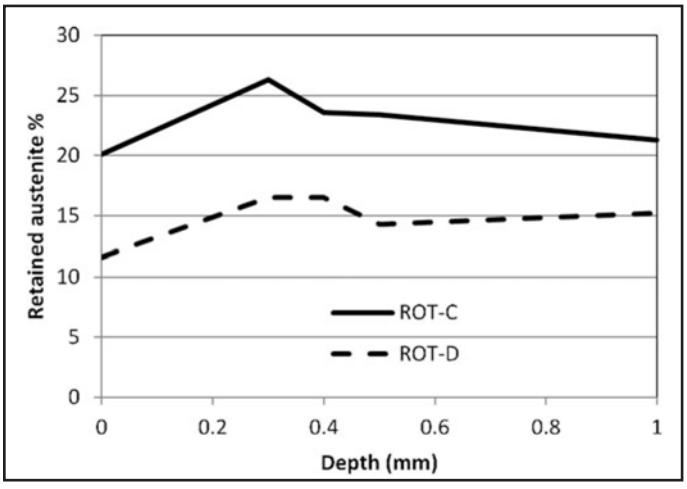

Figure 10 Retained austenite for rotor bearings.

Figure 11 irWEAs on rotor bearing ROT–D IR.

Conclusions

The following conclusions are drawn from field experience working with operating wind turbines that compares the performance of through-hardened and carburized, intermediate bearings, and two rotor bearings with different carburized metallurgies. The conclusions are intended to apply to wind turbine gearbox bearings. They may — or may not — apply to other applications.

Through-hardened bearings fail by axial cracks; carburized bearings fail by macropitting.

Through-hardened bearings display irWEAs on axial cracks that propagate radially through the bearing IR section.

Carburized bearings are more durable in the wind turbine environment than through-hardened bearings, and might be immune to irWEAs and the axial crack failure mode if they have at least 20% retained austenite.

Carburized bearings with less than 20% retained austenite display irWEAs on crack networks that occur over large subsurface areas at depths ranging from the near surface to the depth of the maximum shear stress. When the cracks reach the surface, they form macropits.

Carburized bearings with at least 20% retained austenite might be immune to irWEAs and avoid premature macropitting. **PTE**

Acknowledgement. *The authors express their deepest appreciation to Tibor Tallian for his many helpful suggestions.*

References

1. Warhapande, A., F. Sadeghi and R.D. Evans. "Microstructural Alterations in Bearing Steels under Rolling Contact Fatigue Part 1—Historical Overview," *Tribology Transactions*, 56, 3, 2013, pp 349–358.
2. Gentile, A. J., E.F. Jordan and A.D. Martin. "Phase Transformation in High-Carbon, High-Hardness Steels under Contact Loads," *AIME Transactions*, 233, 1965, pp. 1085–1093.
3. Martin, J. A., S.F. Borgese and A.D. Eberhardt. "Microstructural Alterations of Rolling-Bearing Steel Undergoing Cyclic Stressing," *Journal of Basic Engineering*, 88, 1966, pp 555–567.
4. O'Brien, J. L. and A. H. King. "Electron Microscopy of Stress-Induced Structural Alterations Near Inclusions in Bearing Steels," *Journal of Basic Engineering*, 88, 1966, pp 568–572.
5. Swahn, H., P.C. Becker and O. Vingsbo. "Martensite Decay During Rolling Contact Fatigue in Ball Bearings," *Metallurgical Transactions A*, 7(8), 1976, pp 1,099–1,110.
6. Voskamp, A. P., R. Osterlund, P.C. Becker and O. Vingsbo. "Gradual Changes in Residual Stress and Microstructure during Contact Fatigue in Ball Bearings," *Metals Technology*, 7, 180, 1980, pp 14–21.
7. Zwirlein, O. and H. Schlicht. "Rolling Contact Fatigue Mechanisms — Accelerated Testing vs. Field Performance," *Rolling Contact Fatigue Testing of Bearing Steels*, Hoo, J. J.C., Ed., ASTM, Philadelphia, 1982, pp 358–379.
8. Voskamp, A. P. "Material Response to Rolling Contact Loading," *Transactions of the ASME*, 107, 1986, pp 359–366.
9. Schlicht, H., E. Schreiber and O. Zwirlein. "Effects of Material Properties on Bearing Steel Fatigue Strength," *Effect of Steel Manufacturing Processes on the Quality of Bearing Steels,* ASTM 987, J. J. C. Hoo, Ed., ASTM, Philadelphia, 1988, pp 81–101.
10. Grabulov, A., R. Petrov and H.W. Zandbergen. "EBSD Investigation of the Crack Initiation and TEM/FIB Analyses of the Microstructural Changes around the Cracks Formed under Rolling Contact Fatigue (RCF)," *International Journal of Fatigue*, 32 (3), 2010, pp 576–583.
11. Lund, T. B. (2010), "Sub-Surface-Initiated Rolling Contact Fatigue—Influence of Non-Metallic Inclusions, Processing History, and Operating Conditions," *Journal of ASTM International*, 7(Ref. 5), 2010, pp 81–96.
12. Lund, T. B. "Subsurface-Initiated Rolling Contact Fatigue — Influence of Non-Metallic Inclusions, Processing History and Operating Conditions," *Journal of ASTM International*, **7** (Ref. 5), 2010, pp 81–96.
13. Evans, M. H. "White Structure Flaking (WSF) in Wind Turbine Gearbox Bearings: Effects of 'Butterflies' and White Etching Cracks (WECs)," *Materials Science and Technology*, 28 (Ref. 1), 2012, pp 3–22.
14. Evans, R. D. "Classic Bearing Damage Modes (2011)," Available at *http://www.nrel.gov/wind/pdfs/2011 wind turbine tribology seminar.pdf.*
15. Bohmer, H. J. "Rolling Contact Fatigue," Publication No. WL 40 205 EA, 1993.
16. Hiraoka, K., M. Nagao and T. Isomoto. "Study on Flaking Process in Bearings by White Etching Area Generation," *Bearing Steel Technology — Advances and State of the Art in Bearing Steel Quality Assurance*, Beswick, J. M. Ed., 2007, pp 234–240, ASTM, Philadelphia.
17. Gegner, J. and W. Nierlich. "The Bearing Axial Cracks Root Cause Hypothesis of Frictional Surface Crack Initiation and Corrosion Fatigue-Driven Crack Growth," 2011, Available at *http://www.nrel.gov/wind/pdfs/2011 wind turbine tribology seminar.pdf.*
18. Harada, H. et al. "Microstructural Changes and Crack Initiation with White Etching Area Formation under Rolling/Sliding Contact in Bearing Steel," *ISIJ International*, 45 (12), 2005, pp 1897–1902.
19. Vegter, R. H. and J.T. Slycke. "The Role of Hydrogen on Rolling Contact Fatigue Response of Rolling Element Bearings," *Journal of ASTM International*, 7(2), 2010, pp 1–12.
20. Holweger, W. "Influence on Bearing Life by New Material Phenomena," Available at *http://www.nrel.gov/wind/pdfs/2011 wind turbine tribology seminar.pdf,* 2011.
21. Luyckx, J. "Hammering Wear Impact Fatigue HypothesisWEC/irWEA Failure Mode on Roller Bearings," Available at *http://www.nrel.gov/wind/pdfs/2011 wind turbine tribology seminar.pdf.*
22. Uyama, H. "The Mechanism of White Structure Flaking in Rolling Bearings," Available at *http://www.nrel.gov/wind/pdfs/2011 wind turbine tribology seminar.pdf.*
23. Doll, G. L. "Tribological Challenges in Wind Turbine Technology," Available at *http://www.nrel.gov/wind/pdfs/2011 wind turbine tribology seminar.pdf.*
24. Forster, N., L. Rosado, W.P. Ogden and H. Trivedi. "Rolling Contact Fatigue Life and Spall Propagation Characteristics of AISI M50, M50NiL and AISI 52100, Part III, Metallurgical Examination," *Tribology Transactions*, 53 (Ref. 1), 2009, pp 52–59.
25. Errichello, R. "Microstructural Alterations in Hertzian Fatigue," Available at *http://www.nrel.gov/wind/pdfs/2011 Wind Turbine Tribology seminar.pdf.*
26. Olver, A. "Microstructural Alteration in Rolling Contact," Available at *http://www.nrel.gov/wind/pdfs/2011 wind turbine tribology seminar.pdf.*

Robert Errichello heads his own gear consulting firm—GEARTECH—and is a founder of GEARTECH Software, Inc. He is a registered professional engineer and a graduate of the University of California at Berkeley. He holds B.S. and M.S. degrees in mechanical engineering and a master of engineering degree in structural dynamics. Errichello has over 34 years of industrial experience and has worked for several gear companies. He has been a consultant to the gear industry for the past 19 years; has taught courses in material science, fracture mechanics, vibration and machine design at San Francisco State University and the University of California at Berkeley; and is a member of ASM International, STLE, ASME Power Transmission and Gearing Committee, AGMA Gear Rating Committee and the AGMA/AWEA Wind Turbine Committee. Errichello has published over 40 articles on design, analysis and the application of gears and is the author of three widely used computer programs for the design and analysis of gears. He is a technical editor for Gear Technology magazine and STLE Tribology Transactions and has presented numerous seminars on design, analysis, lubrication and failure analysis of gears. Errichello is a recipient of the AGMA TDEC Award and the STLE Wilbur Deutch Memorial Award.